FBG based seismic vibration sensor with inverted spring-mass system

PUTHA KISHORE[*]
Department of Physics, National Institute of Technology Warangal, India

In this paper, we report the design of an FBG based seismic vibration sensor with an aid of an inverted spring-mass system to sense the primary waves of seismic vibration. A simple linear edge filter also designed using simple Single mode – Multimode - Single mode (SMS) configuration to interrogate the FBG. The obtained experimental results show that the proposed sensor is capable to measure the frequency of vibrations over the span of 2-20Hz. It is also evident that the designed sensor exhibits high sensitivity at 7.5Hz, which represents the resonance frequency of the sensor. The sensor parameters cane be alter by choosing the spring mass system parameters and the position of the FBG attached between the spring and the post.

1. Introduction

A seismometer or seismic sensor detects, amplifies, and records earthquakes as well as other ground motion of the structures. In general seismic sensor refers to a transducer, which is based on a mass which is attached to the transducer base, usually with a linear spring. The base is attached to the surface whose motion is to be detected, and the motion of the seismic mass relative to the base is sensed by the transducer. As the system vibrates, the mass tends to remain fixed to its position so that the motion can be registered as a relative displacement between the inertial mass and the frame [1-4]. A variety of seismic sensors have been employed to sense the movement of the inertial mass of the relative ground motion. These involve a diverse type of sensors, whose characteristics are classified mainly as either mechanical, electromechanical, electromagnetic, electrical or optical depending upon the restoring force or other measuring mechanism. The mechanical sensors use the mechanical properties like the laws of motion, distortion of spring or fluid dynamics to measure the seismic vibration. The mechanical elements used to fabricate these sensors are inferior for the reason of friction at constant points, such as a stylus that records on a blackened drum [2, 5]. The electromechanical transducer is a part in the seismic instrument, which gives an output proportional to the ground motion, and is measured using suitable electronic circuitry whose output follows proportional to the velocity of the ground motion in an inertial frame. The most widely used and successful electromagnetic seismic sensor is one that employs a coil of wire and a magnet. The magnet is fixed to the base of the sensor, and the coil moves with inertial mass. The relative motion causes the magnetic flux through the coil to change in time that generates a voltage which is proportional to the velocity of the mass [1, 2]. As compared to the measurement of the position of the mass, velocity measurement is a poor choice for those concerned with improving low-frequency performance. In most modern electrical seismometers, a capacitor or a MEMS, or a piezoelectric, or an LVDT has been used as a sensitive element in differential configuration that change in the opposite manner in response to mass motion [6-10]. Latter, advanced and emerging techniques are developed using optical methods. One of the optical techniques is laser interferometry, which is based on Michelson interferometer. The main limitations of this sensor are environmental parameters [11]. To overcome all these drawbacks optical fiber based sensors have been introduced into seismic sensing applications due to their inherent advantages.

In general, seismic sensors have the limitation in frequency range, because of their complete dependence on mechanical design and sensing principle. The band of frequencies interested in seismic applications are of the very large range, from 5 to 1000Hz. Till now, there is no single instrument covering this entire wide range, and instruments with different range of gain and frequency response are used for different ranges of frequencies and amplitudes. The challenge is therefore to construct seismic sensors, which cover at least a large part of the above range [1].

Generally in seismic vibration, the release of the stored energy is caused by sudden fracture and movement of rocks inside the earth. Part of the energy released produces seismic waves like Primary (P), Secondary (S) and Surface waves that travel outward in all directions from the point of initial rupture. These waves shake the ground as they pass by. P-wave is the first seismic wave detected by seismographs as it is the fastest wave, able to

move through both liquid and solid bodies. Seismic waves are also called compression or longitudinal waves, they compress and expand the ground back and forth in the direction of travel, similar to sound waves that move back and forth as the waves travel from source to receiver. The S-wave oscillate the ground perpendicular to the direction of the motion. That is S-wave can produce vertical and horizontal motion on the ground surface. In general, S-waves travel about 1.7 times slower than P-waves. Because liquids will not sustain shear stresses, S-waves cannot travel through liquids. The surface wave moves close to or on the outside surface of the ground rather than through the deep interior like a P or S waves [12-13]. Several optical fiber based methods have been proposed in the literature, mainly based on FBG sensors to measure the seismic vibration [14-17]. Most of these sensors are suitable to measure the S-wave vibration only.

However, this paper presents a novel attempt to design and demonstrate a simple FBG based seismic vibration sensor to sense the P-wave or horizontal vibration only with an aid of inverted spring mass sytem, some of the results of the proposed work are already presented [17]. Also, a simple FBG interrogation is implemented using SMS configuration for converstion of wavelength coding to internsity modulation.

2. Theory of FBG

In its simplest form, an FBG consists of a periodic modulation of the refractive index in the core of a single-mode optical fiber. Generally, in uniform fiber gratings, the phase fronts are perpendicular to the longitudinal axis of the fiber and the grating planes are of a constant period [18-20]. These are considered as the fundamental building blocks of the most Bragg grating structures. Light guided along the core of an optical fiber is scattered by each grating plane. When the Bragg condition is not satisfied, the reflected light from each of the subsequent planes become progressively out of phase and will eventually get cancelled out. Additionally, light that is not coincident with the Bragg resonance wavelength will experience very weak reflection at each grating plane because of the phase mismatch. When the Bragg condition is satisfied, the contributions of reflected light from each grating plane is added constructively in the backward direction to form a back-reflected peak with the center wavelength defined by the grating parameters. The Bragg grating condition is simply the requirement that satisfies both energy and momentum conservation. Energy conservation ($\hbar\omega_f = \hbar\omega_i$) requires the frequency of the incident radiation and the reflected radiation be the same. Momentum conservation requires that the sum of incident wave vector (k_i) and the grating wave vector (K) should be equal to the wave vector of the scattered radiation (k_f). This can be expressed as

$$k_i + K = k_f \tag{1}$$

where, the grating wave vector K has a magnitude $2\pi/\Lambda$, in the direction normal to the grating planes, and Λ is the grating spacing or pitch. The diffracted wave vector is equal in magnitude but opposite in direction to the incident wave vector. Hence, the momentum conservation condition becomes

$$2\left(\frac{2\pi n_{eff}}{\lambda_B}\right) = \frac{2\pi}{\Lambda} \tag{2}$$

This simplifies to the first order Bragg condition

$$\lambda_B = 2n_{eff}\Lambda \tag{3}$$

Assuming a uniform Bragg grating formed within the core of an optical fiber with an average refractive index n0, the refractive index profile can be expressed as

$$n(z) = n_0 + \Delta n \cos\frac{2\pi z}{\Lambda} \tag{4}$$

where, Δn is the modulation amplitude (typically 10^{-5} to 10^{-3}) and z is the axial position.

2.1. Sensing principle of FBG

This section describes some applications of the FBG. The Bragg wavelength of FBG strongly depends on the local temperature and strain. The Bragg wavelength shift occurs due to changes in n_{eff} and/or Λ of the FBG which are effected by strain and temperature as given below [18-21].

$$\Delta\lambda_B = 2\left(\Lambda\frac{\partial n_{eff}}{\partial l} + n_{eff}\frac{\partial\Lambda}{\partial l}\right)\Delta l + 2\left(\Lambda\frac{\partial n_{eff}}{\partial T} + neff\partial\Lambda\partial T\Delta T\right) \tag{5}$$

where T is temperature, l is the grating length, $\Delta\lambda_B$ is the change in Bragg wavelength, Λ is the pitch of the grating and neff is the effective refractive index. The first term in equation 4 represents the strain effect on a Bragg grating, because strain causes a change in Λ and n_{eff}. Therefore, strain effect can be represented as
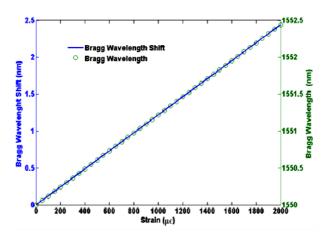
$$\Delta\lambda_B = \lambda_B(1 - p_e)\epsilon_z \tag{6}$$

The term ϵ_z is an axial strain experienced by the optical fiber at an FBG location in micro-strain ($\mu\epsilon$) along the axis, and p_e is the effective photo-elastic constant of the fiber material, which is defined as

$$p_e = \frac{n_{eff}^2}{2}[p_{12} - \upsilon(p_{11} + p_{12})] \tag{7}$$

where p_{11} and p_{12} are components of the strain-optic tensor, and υ is the poison's ratio. Fig. 1(a) shows the variation of $\Delta\lambda_B$ with the increase in strain in the FBG, for a typical Germanosilicate optical fiber, p_{11}=0.113, p_{12}=0.252 and $\upsilon = 0.16$ and $n_{eff} = 1.482$. The strain sensitivity of the FBG at 1550nm is 1.2pm of wavelength shift for 1$\mu\epsilon$ applied to the grating.

The second term in equation 5 represents the effect of temperature on the spectral response of Bragg grating. Bragg wavelength shift in this case is due to a change in Λ and n_{eff}.
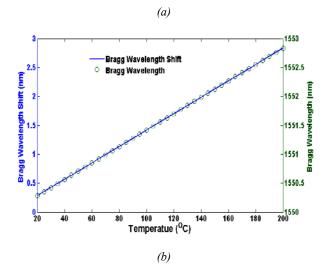

(a)

(b)

Fig. 1. Shift in Bragg wavelength with applied a) axial strain b) temperature on a uniform grating of length 3mm.

The thermal term can be represented as

$$\Delta\lambda_B = \lambda_B(\alpha + \zeta)\Delta T \qquad (8)$$

where $\alpha = \frac{1}{\Lambda}\frac{\partial \lambda}{\partial T}$ is the thermal expansion coefficient for the fiber ($0.55 \times 10^{-6}/^{\circ}C$ for silica). The second term $\zeta = \frac{1}{n_{eff}}\frac{\partial n_{eff}}{\partial T}$ is the thermo optic coefficient and its value for Germania doped silica core fiber is approximately $8.6 \times 10^{-6}/^{\circ}C$. Fig. 1(b) shows the variation of $\Delta\lambda_B$ with the increase in temperature of the FBG. The resultant temperature sensitivity of the FBG at 1550nm is found to be 14pm of wavelength shift for $10^{\circ}C$ rise in temperature. From equations 4, 5 and 8, it is apparent that the wavelength response of the Bragg grating is dependent on both temperature and strain. Bragg gratings are quite useful as passive sensors for structural monitoring, where the gratings may be multiplexed into a fiber, allowing multi-point sensing information to be monitored.

3. Discrimination between temperature and seismic vibration

The shift in Bragg wavelength of the FBG indicates the effect of both vibration (strain) and temperature. In general, the common method to discern them is using another reference FBG (FBG1), being in thermal contact with the sensing FBG (FBG2), and is shielded from the applied vibration. When the FBG sensor is subjected to vibration or ambient temperature change, the effective refractive index and the grating pitch will change, which in turn creates a shift in resonance wavelength. The shift of resonance wavelengths for FBG1 and FBG2 can be expressed as [24, 25]

$$\Delta\lambda_{B1} = J_{S1}\Delta S + J_{T1}\Delta T \text{ and } \Delta\lambda_{B2} = J_{S2}\Delta S + J_{T2}\Delta T \qquad (9)$$
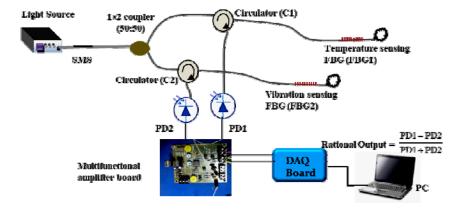

Fig. 2. Illustrates a schematic diagram of the experimental setup to discriminate the temperature from seismic vibration

where $J_{S1}, J_{T1}, \; J_{S2}$ and J_{T2} are strain and temperature sensitivity coefficients of FBG1 and FBG2 respectively. From equation (8), when strain and temperature changes, the strain can be obtained on the basis of subtracting the Bragg wavelength shift induced by the reference FBG (FBG1) from the total wavelength shift induced by the sensing FBG (FBG2).

To realize the simultaneous measurement of strain and temperature, the Bragg wavelength shift of two resonant peaks of corresponding FBGs need to be measured simultaneously. In this way, discrimination between strain and temperature can be achieved by the following matrix equation

$$\begin{bmatrix} \Delta S \\ \Delta T \end{bmatrix} = \frac{1}{\psi} \begin{bmatrix} J_{T2} & -J_{T1} \\ -J_{S2} & J_{S1} \end{bmatrix} \begin{bmatrix} \Delta \lambda_{B1} \\ \Delta \lambda_{B2} \end{bmatrix} \qquad (10)$$

where $\psi = J_{S1}J_{T2} - J_{S2}J_{T1}$, strain and temperature sensitivity coefficients can be determined experimentally by measuring the Bragg wavelength shift of the FBGs separately.

This technique is suitable only for slow and manual measurement systems. Whereas it is not applicable for fast and real time monitoring applications, and also to the intensity modulated interrogation system based sensors, because the equation (9) is having the matrix with Bragg wavelength shift coding. However the proposed sensor is interrogated to convert the wavelength information into intensity modulation. In order to overcome this difficulty a simple method is proposed to discriminate the temperature from vibration (strain).
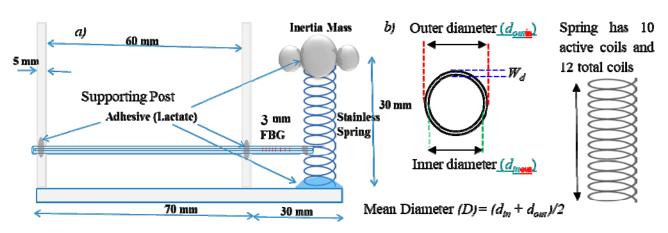

Fig. 3. (a) Schematic of the seismic vibration sensor and (b) spring specifications

The light from a broadband light source (BBLS) will be modulated by single mode - Multimode - Single mode (SMS) fiber and then is allowed to illuminate two similar FBGs through 1×2 (50:50) coupler and optical circulators (C1 and C2). The light reflected from the FBGs are detected by the corresponding photo-detectors PD1 and PD2. To avoid the effect of source signal power variation and ambient temperature on sensing, an all-fibre ratiometric power measurement technique can be used. Otherwise, the difference between the output powers of the PD1 and PD2 corresponding to the FBG's gives the response of only seismic vibration.

4. FBG seismic vibration sensor design

In general seismic vibrations are the dynamic deformations of the earth or structure, which are generally monitored and controlled or recorded from a remote location. Fiber optic sensors are well suitable for such kind of applications due to their inherent advantages. The schematic structure of the sensor head includes FBG attached to the spring with specifications is shown in Fig.

3. The sensor is designed using inverted spring holding the inertial mass and arranged in such a way that it produces vibration in the axial direction to that of the optical fiber, which are similar to the primary wave of seismic vibration. Therefore, the designed sensor system with simple mechanical construction will allow the major movement in one direction only. The axial seismic vibration of the body is measured by measuring the axial strain produced by the FBG with respect to oscillatory motion of the spring-mass system. The frequency response of the sensor system depends on two factors. The first dominant and important factor is the natural frequency f_k of the spring-mass system which can be obtained by the following equation [26, 27],

$$f_k = \frac{1}{2\pi} \sqrt{\frac{k}{m}} \qquad (11)$$

where m is the mass suspended by the spring and k is the spring constant which depends on spring coil properties expressed as [26]

$$k = \frac{G W_d^{\,4}}{8nD^3} \tag{12}$$

Here $W_d = 0.5$mm is wire diameter, $D = 7.7$mm is the mean diameter of the spring, $n = 10$ is the number of active coils and G=11.2 Mpsi is the shear modulus of stainless steel. From this data the calculated spring constant is obtained as k=0.135 N/mm. For the inertial mass of 3gm glued on the overhead of the spring, the natural frequency of the designed spring-mass system is calculated as 33.72Hz using equations (11) and (12).

The second factor is the intrinsic resonance frequency of the optical fiber and is described as [28-29]

$$f_o = \frac{1}{2\pi} \sqrt{\frac{2k_f}{m_t}} \tag{13}$$

where k_f is the spring constant of the quartz fiber, which depends on the area and the length of the optical fiber used, and it can be expressed as

$$k_f = \frac{E\,A}{l} \tag{14}$$

Here E is the elastic modulus of quartz fiber (73×10^9 N/m), $A = \pi \left(\frac{d}{2}\right)^2$ is the cross sectional area of the fiber (12.27×10^9 m^2), d is diameter is typically 125μm), l=10mm is the length of the fiber attached between the supporting posts and spring, where inscribed a 3mm length of FBG at 1549nm is used for the sensing purpose, and m_t the total inert mass of 3.5gm (spring and inertial mass). From equations (13) and (14), the computed intrinsic resonance frequency of the optical fiber is 780Hz. The obtained resonance frequencies of the sensor system limits the maximum measurable frequency up to 33.72Hz only; because it is the lowest value of above two. Here the resonance conditions are measured independently, and may not give the exact value of the resonance frequency of the complete system but one can estimate the limit.

5. Interrogation of the FBG using SMS structure

In general FBG gives the wavelength shift corresponding to change in strain/vibration or temperature. Particularly, real time monitoring applications such as vibration, requires fast and high resolution interrogation system. Aiming to attribute this a simple, high speed and cost effective integration scheme using Single mode-Multimode-Single mode (SMS) configuration is designed and demonstrate experimentally. The formation of fiber edge filter using SMS configuration to match with the Bragg wavelength of FBG can be optimized by changing the length of the multimode fiber [30-34]. The design of SMS fiber structure encompasses the splicing of a step-index multimode fiber (MMF) between two standard

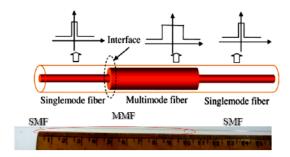single mode fibers (SMF-28e). The schematic of the SMS fiber structure is shown in Fig. 4.

Fig. 4. Photograph of the designed single mode–multimode–single mode fiber structure

The working principle of linear edge filter can be described as follows: the light field propagating along the input SMF enters into the MMF section and excites a number of guided modes in the MMF. Consequently the interference between the different modes occur while the light field propagates through the MMF section. By choosing a suitable length for the MMF section, the light coupled into the output end of the SMF can be made as wavelength dependent due to the interference. When input field is applied from SMF to MMF, a specific number of guided modes are excited inside the MMF. However, the power coupling efficiency is maximum only for a specific mode number, which depends on the fiber properties and especially on the fiber diameter. Whereas, the coupling efficiency to the output SMS depends on the length of the MMF only. Therefore, the coupling loss of the SMS structure depends strongly on the length of the MMF. However, it is also wavelength sensitive which can be easily predicted from the length of MMF. Therefore, the SMS fiber structure act as either band-pass filter or edge filter depending on the length of the MMF.
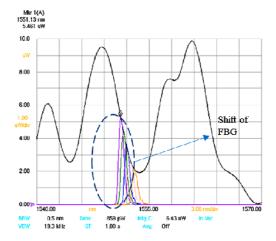

Fig. 5. OSA spectrum of the designed SMS configuration for Interrogation

The standard single mode fiber (SMF-28e) with refractive indices of the core (9μm) and cladding (125μm) given as 1.4502 and 1.445 respectively at the wavelength

of 1550nm has been employed for the input and output fibers. The MMF employed has the corresponding core and cladding refractive indices as 1.47 and 1.45 respectively, with the diameter of the core/cladding given by 100/125μm. As already discussed transmission spectrum of the SMS is strongly dependent on the length of the MMF and it determines the operating wavelength range of the filter [35-37]. The transmission spectrum of the designed SMS structure for optimized length of 10cm MMF is shown in Fig. 5. This band-pass characteristic of SMS exhibits a linear edge filter response on either side of the center wavelength at 1553.75nm. Consequently, this device can be used as an edge filter over a selected wavelength range centered around 1553.75nm. Therefore the (negative slope) region between 1548 and 1553 nm has been selected in the present investigation to interrogate the FBG (Bragg wavelength at 1551nm) response corresponding to seismic vibration. Fig. 5 also projects the optical intensity modulation related to the shift in Bragg wavelength of FBG corresponding to seismic vibration.
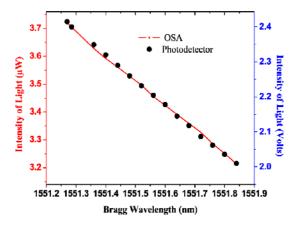

Fig. 6. The interrogation results of the FBG using SMS configuration

A simple two channel photo-detector along with the transimpedance amplifier circuit is used to convert the detected optical intensity information into a readable voltage signal. Fig. 6 illustrates the Bragg wavelength shift and power variation of the FBG through SMS linear edge filter response corresponding to seismic strain which is recorded using OSA. Fig. 6 also shows the equivalent optical intensity modulation in terms of voltage obtained by the photo-detection system. From the above results it is observed that the experimental results obtained using both OSA and designed detection system of the interrogator are well coinciding with a linearity coefficient of 99%.

6. Experimental setup

The schematic experimental setup of the FBG based seismic vibration sensor is shown in Fig. 7. The light from the broadband source (Thorlabs-S51005S) having peak wavelength at 1540nm is coupled to SMS interrogator and then transmitted to port1 of the circulator. The light from

the port1 of the circulator is directed towards port2 and transmitted through FBG. The reflected Bragg wavelength from the FBG is directed towards port3, is then allowed to be incident on the photo-detector (DPIN-23113). The transimpedance amplifier circuit converts the detected light into its equivalent voltage signal. This signal is then collected by the NI-DAQ and is monitored and processed by LabVIEW program, which is programed in a PC for the analysis of seismic vibration. A synthesized signal generator (HM8130) is used to vibrate the designed seismic vibrator at different frequencies with variable amplitude.

FBG of length 3mm having peak wavelength at 1551nm has been used as a sensor in the present experimental work. The FBG is fixed between the supporting post and fourth turn of the helical spring (at a height of 9.5mm from the base) as shown in Fig. 3. Further, the wavelength encoded information corresponding to seismic vibration is converted into equivalent electrical signals using the interrogation scheme as discussed in previous report [38].
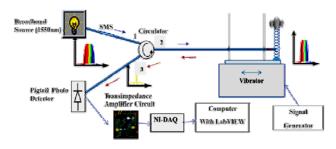

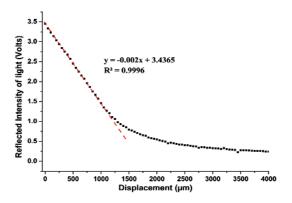*Fig. 7. Schematic experimental setup of the seismic vibration sensor*

Fig. 8. Displacement response of the vibrator using dual fiber optic sensor for calibration of the seismic sensor

7. Results and discussions

To study the response of the sensor, the sensor head is mounted on a specially designed seismic vibrator which is controlled by the signal generator. The vibrator is calibrated using dual plastic optical fiber vibration acceleration amplitude of 0.078g. Fig. 11 represents the amplitude response of the sensor at constant frequency of

7.5Hz for varying acceleration amplitudes. It illustrates that the sensor amplitude response is linear with respect to the applied amplitude of vibration. The frequency response of the FBG seismic sensor reveals that there is a good agreement between the applied and measured frequencies in the range of 2-20Hz. Below 2Hz the seismic vibration system (spring-mass system) is not showing any oscillatory motion due to its inertial mass. Above 2Hz the sensor response quite good up to 20Hz which is considered as upper limit of the proposed sensor. Therefore, experimental results reveal that the combined system can be used to sense frequencies up to 20Hz.This is due to the fact that the theoretical resonance frequency of optical fiber and spring mass system are limited to 780Hz and 34Hz respectively. The amplitude response of the sensor has also been tested at constant frequency of 7.5Hz and is shown in Fig. 12. The amplitude response of the sensor at different frequencies and it is found that there is a linear relationship between the applied and measured amplitude of vibration is shown in Fig. 13(a).
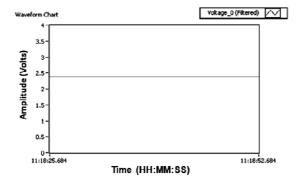

Fig. 9. Time domain signal of the FBG seismic sensor without any vibration
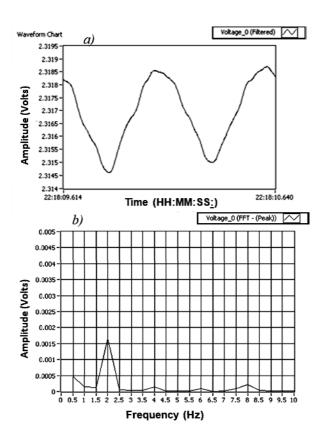

Fig. 10. (a) Time domain signal and (b) corresponding FFT spectrum of the FBG seismic sensor at 2Hz frequency of vibration
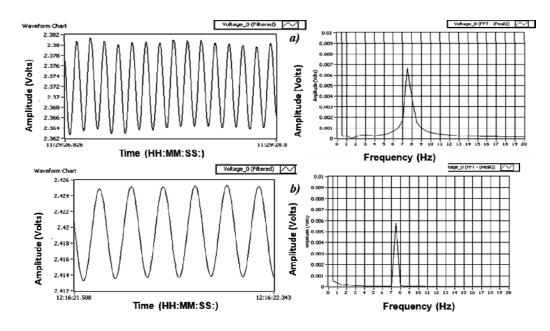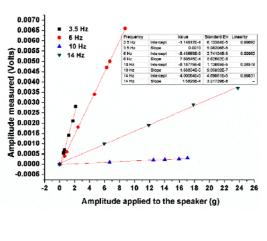

Fig. 11. Response of the sensor at constant frequency of 7.5Hz for varying amplitudes of a) 0.0065g and b) 0.0052g

The amplitude sensitivity of the sensor at constant frequency is measured by applying variable amplitude of vibration and noting the corresponding response by the sensor. The same experiment is repeated at different frequencies and measured the amplitude sensitivities, and then the characteristic curve between the amplitude sensitivity and frequency is plotted as shown in Fig. 13(b). From this, it is observed that at a frequency of 7.5Hz the sensor shows high sensitivity, which represents the resonance frequency of the sensor system. The resonance frequency and the frequency range of the sensor can be changed by varying the parameters of the optical fiber or spring-mass system and also the position (height from the base) of the FBG attached to the spring. As already mentioned that, the Bragg wavelength shift in FBG may be due to the change in either temperature or strain and or both. Here, the intension of the sensing parameter is only a strain and which is developed in the FBG with respect to the seismic vibration. Thus, the discrimination of the temperature from strain is very important task, which can lead to simultaneous measurement of vibration and temperature as well as discrimination between them.
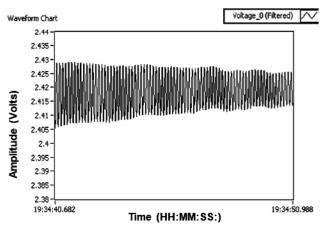

Fig. 12. Continuous varying amplitude response at constant frequency of 7.5Hz.
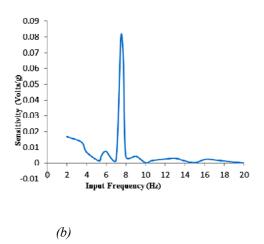

(a)

(b)

Fig. 13. (a) Amplitude response of the sensor at different frequencies and (b) Amplitude sensitivity corresponding to the frequency characteristic curve of the sensor.

8. Conclusions

An attempt had been made to design the FBG based seismic vibration sensor using an inverted spring-mass system. The sensor is configured using a vertical spring glued with overhead weight that provides damped motion of the spring in the axial direction with respect to the seismic vibration (P-wave). An interrogation system is developed using SMS structure to monitor the Bragg wavelength shift of FBG in terms of optical intensity modulation corresponding to the seismic vibration. The experimental results show that the proposed sensor is capable to measure the frequency of vibrations over the span of 2-20Hz. It is also evident from the results that the sensor is highly sensitive at 7.5Hz, which represents the resonance frequency of the designed sensor. The

frequency of resonance and range of frequency can be varied by changing the spring parameters or overhead weight and also the position of the FBG attached between the spring and the post. The discrimination of the temperature from the seismic vibration is also discussed to eliminate the effect of temperature on sensing and also to monitor the temperature and vibration simultaneously.

References

[1] J. G. Webster, Measurement, Instrumentation, and Sensors Handbook, CRC Press LLC, Ch. 16 and 17, 1999.
[2] H. Jens, G. Alguacil, Instrumentation in earthquake seismology, Springer Publisher, Netherlands, 2010.

[3] E. Wielandt's, Seismic sensors and their calibration, New Manual of Seismological Observatory Practices, 1-46, 2009.

[4] C. Collette, S. Janssens, P. Fernandez-Carmona, K. Artoos, M. Guinchard, C. Hauviller, A. Preumont, Bull. Seism. Soc. Am. **102**(4), 289 (2012).

[5] F. Acernese, R. de Rosa, F. Garufi, G. Giordano, R. Romano, F. Barone, Journal of Physics: Conference Series, **228**(1), 012035 (2010).

[6] W. Clarence, De Silva, Earthquake Engineering & Structural Dynamics **8**(4), 337 (1980).

[7] Alex Pakhomov, Tim Goldburt, Defence and Security, International Society for Optics and Photonics, 463 (2004).

[8] A. Pakhomov, D. Pisano, A. Sicignano, T. Goldburt, Defence and Security, International Society for Optics and Photonics, 422 (2005).

[9] A. Pakhomov, A. Sicignano, M. Sandy, T. Goldburt, Defence and Security, International Society for Optics and Photonics, 576 (2004).

[10] A. Neylon, MEMS based seismic and vibration sensor in Building & Structural Health Monitoring Systems, MEMSCON Workshop, Bucharest, 7th Oct. 2010.

[11] A. Fausto, R. de Rosa, F. Garufi, R. Romano, F. Barone, International Society for Optics and Photonics **9061**, 90612H-1 (2007).

[12] Y. Bozorgnia, V. Bertero, Earthquake engineering: from engineering seismology to performance-based engineering, CRC Press LLC, New York Washington, D.C., 33 (2004).

[13] P. M. Shearer, Introduction to seismology, Cambridge University Press, New York, 2009.

[14] Y. Zhang, S. Li, Z. Yin, R. Pastore, K. O'Donnell, M. Pellicano, J. Kosinski, H.-L. Cui, Proc. of SPIE **5855**, 1008(2005).

[15] Y. Zhang, S. Li, R. Pastore, Z. Yin, H.-L. Cui, Proc. of SPIE **6371**, 63710R-1(2006).

[16] Y. Weng, X. Qiao, T. Guo, M. Hu, Z. Feng, R. Wang, J. Zhang, IEEE Sensor **12**(4), 2011.

[17] D. Dinakar, P. Kishore, P. Vengal Rao, K. Srimannaraynan, SPIE Conf. Proc. 9141-65 (2014).

[18] Andreas Othonos, Kyriacos Kalli, Fiber Bragg Gratings: Fundamentals and Applications in Telecommunications and Sensing, Artech House, Boston, London, 1999.

[19] Raman Kasyap, Fiber Bragg Gratings, Academic Press, San Diego, 1999.

[20] Y.-J. Rao, Meas. Sci. Tech. **8**, 355 (1997).

[21] X. Zhang, J. Zhao, Y. Huang, X. Ren, International conference on Communication Technology Proceedings, Beijing, China, 2003.

[22] H. O. Kenneth, B. Malo, F. Bilodeau, D. C. Johnson, J. Albert, App. Phys. Let. **62**(10), 1035(1993).

[23] N. Singh, S. C. Jain, A. K. Aggarwal, R. P. Bajpai, J. of Sci. and Ind. Research **64**, 108 (2005).

[24] M. Xu, J. L Archambault, L. Reekie, J. P. Dakin, Elec. Lett. **30**, 1085 (1994).

[25] P. Saidi Reddy, R. L. N. Sai Prasad, D. Sengupta, M. Sai Shankar, K. S. Narayana, Micro. and Opt. Tech. Lett. **53**(5), 1021(2011).

[26] S. Timoshenko, D. H. Young, Vibration Problems in Engineering, Nostrand Company, D. Van, Inc., Third Edition, New York, 1, 1955.

[27] T. A. Berkoff , A. D. Kersey, IEEE Photonics Tech. Lett. **8**(12), 1677 (1996).

[28] Sun Ru-Jiao, Sun Li-min, Sun Zhi, Dan Dan-Hui, Liu Xio-hui, Acta Photonica Sinica **36**(1), 63 (2007).

[29] Y. Zhang, S. Li, Z. Yin, R. Pastore, K. O'Donnell, M. Pellicano, J. Kosinski, H.-L. Cui, Proc. of SPIE **5855**, 1008 (2005).

[30] Qiang Wu, Agus Muhammad Hatta, Yuliya Semenova, Gerald Farrell, Appl. Opt. **48**(29), 5451 (2009).

[31] Q. Wang, G. Farrell, Micro. and Optitech. Let. **48**(5), 900 (2006).

[32] M. S. Waleed, Alok Mehta, E. G. Johnson, J. of Light. Tech. **22**(2), 469 (2004).

[33] Q. Wang, Gerld Farrell, W. Yan, J. of Light. Tech. **26**(5), 512 (2008).

[34] S. Dipankar, P. Kishore, Opt. Eng. **53**(1), 017102 (2013).

[35] J. Chang, D.-H. Huo, L.-Z. Ma, X.-H. Liu, T.-Y. Liu, C. Wang, J. of Elec. Sci. and Tech. of China **6**(4), 486 (2008).

[36] J.-Y. Wang, T.-Y. Liu, C. Wang, X.-H. Liu, D.-H. Huo, J. Chang, Meas. Sci. Tech. **21**(9), 094014 (2010).

[37] A. Laudati, F. Mennella, M. Giordano, G. D'Altrui, C. Calisti Tassini, A. Cusano, IEEE Photonics Tech. Lett. **19**(24), 1991 (2007).

[38] P. Kishore, D. Dinakar, P. Vengal Rao, K. Srimannarayana, Optica Applicata **43**(4), 793 (2013).

[*]Corresponding author: kishorephd.nitw@gmail.com